Structural and electronic properties of $Co/Al_2O_3/Co$ magnetic tunnel junction from first principles

I. I. Oleinik, E. Yu. Tsymbal, and D. G. Pettifor
Department of Materials, University of Oxford, Parks Road, Oxford OX1 3PH, United Kingdom
(Received 3 December 1999; revised manuscript received 17 March 2000)

A detailed first-principles study of the atomic and electronic structure of the $Co/Al_2O_3/Co$ magnetic tunnel junction has been performed in order to elucidate the key features determining the spin-dependent tunneling. The atomic structure of the multilayer with the O- and Al-terminated interfaces between fcc Co(111) and crystalline α-$Al_2O_3(0001)$ has been optimized using self-consistent spin-polarized calculations within density-functional theory and the generalized gradient approximation. We found that the relaxed atomic structure of the O-terminated interface is characterized by a rippling of the Co interfacial plane, the average Co-O bond length being 2.04 Å which is within 5% of that in bulk CoO. The corresponding electronic structure is influenced by the covalent bonding between the O $2p$ and Co $3d$ orbitals resulting in exchange-split bonding and antibonding states and an induced magnetic moment of $0.07\mu_B$ on the interfacial oxygen atoms. The Al-terminated interface contains Co-Al bonds with an average bond length of 2.49 Å compared to 2.48 Å in bulk CoAl. Due to charge transfer and screening effects the Co interfacial layer acquires a negative charge which results in a reduced magnetic moment of $1.15\mu_B$ per Co atom. We found that the electronic structure of the O-terminated $Co/Al_2O_3/Co$ tunnel junction exhibits negative spin polarization at the Fermi energy within the first few monolayers of alumina but it eventually becomes positive for distances beyond 10 Å .

I. INTRODUCTION

Magnetic tunnel junctions (MTJ's) are promising candidates for applications in spintronic devices such as magnetic random access memories, read heads, and sensors.[1] The MTJ's consist of two ferromagnetic layers separated by an insulating barrier layer. The physical quantity measured for signal detection is the tunneling magnetoresistance (TMR), i.e., the relative difference in the resistance between parallel and antiparallel magnetizations of the electrodes. It was found that the TMR could be as high as 30% at room temperature in tunnel junctions based on ferromagnetic $3d$-metal electrodes when alumina is used as the barrier layer (for a recent review, see Ref. 2).

The magnitude of the TMR is determined by the spin polarization (SP) of the tunneling current, which can be measured in experiments on superconductors.[3] It was generally accepted that the SP of the tunneling current is an intrinsic property of the ferromagnets and is determined by the SP of the electronic density of states (DOS) at the Fermi energy.[4] Experimental results show, however, that the SP of the tunneling current is strongly dependent on the structural quality of the tunnel junctions. Improvements in the quality of the alumina barrier and the metal/alumina interfaces result in an enhancement of the measured values of the SP. For example, the SP of permalloy of 32% was obtained in early experiments on tunneling to superconductors,[3] later this value increased to 48%,[2] and very recently it was found that the SP of permalloy is 57%.[5] Experiments also show that the SP is dependent on the choice of the tunneling barrier. Negative values of the SP were obtained at low applied voltage when tunneling occurs from Co across a $SrTiO_3$ barrier,[6] whereas it is positive across an alumina insulating layer.[3] We see therefore that the SP is *not* an intrinsic property of the ferromagnet alone but depends on the structural and electronic properties of the entire junction including the insulator and the ferromagnet/insulator interface.

This fact is also supported by theoretical investigations of the spin-dependent tunneling (SDT). Early calculations showed that within a free electron model the potential barrier height influences the magnitude and sign of the SP.[7] The SP can also be effected by the actual profile of the potential barrier[8] and the disorder within the insulator.[9,10] The multiband description of the electronic transport problem shows that the SP of the tunneling current depends strongly on the mechanism of bonding at the interface between the ferromagnetic metal and the insulator layer[11] and is characterized by different decay lengths of evanescent Bloch waves through the barrier.[12]

Thus these experimental and theoretical results demonstrate that a realistic description of the atomic and electronic structure of the magnetic tunnel junction is crucial for a quantitative description of the SDT and for an accurate prediction of the TMR. This is a very complicated problem especially due to the *amorphous* structure of the alumina barrier layer. In addition, due to the difficulties in the atomic scale characterization of the magnetic tunnel junctions, there is little direct atomistic information about the structure and bonding at the ferromagnet/alumina interface. This is quite different from the situation with other metal/alumina interfaces so far studied in which the metal is grown on top of *crystalline* Al_2O_3 (see, for example, Ref. 13) making the system tractable by first-principle methods.[14,15]

The primary goal of this work is therefore to make a first step in understanding the properties of $Co/Al_2O_3/Co$ tunnel junctions by addressing the two principal issues: (i) the atomic structure of the MTJ, and (ii) the electronic structure of the MTJ. We consider both Al- and O-terminated inter-

faces in coherent geometries which provide the smallest possible lattice mismatch between bulk fcc cobalt and crystalline α-alumina. Full geometry optimization of the structure is performed by self-consistent spin-polarized calculations within density-functional theory and the generalized gradient approximation using the total-energy plane-wave pseudopotential code *CASTEP*.[16] Although it is possible in principle to calculate the electronic local density of states within plane-wave methods, this is very expensive due to the necessity of sampling *k*-space densely. Therefore the spin-polarized electronic structure of the Co/Al_2O_3 interfaces was studied by means of the scalar-relativistic linear muffin-tin orbital (LMTO) method.[17] We conclude the paper with a discussion of the electronic properties of the $Co/Al_2O_3/Co$ MTJ relevant to SDT.

II. ATOMIC STRUCTURE

We have constructed a realistic model for the atomic structure of the cobalt/alumina/cobalt tunnel junction within a supercell approach by incorporating most of the important features of the real Co/Al_2O_3 thin-film system. What experimental information is available for the case of a cobalt/alumina interface? First, experiments show that in thin films cobalt exists predominantly in the fcc phase. Second, it is known that the alumina grows on top of the (111) plane of fcc cobalt which exhibits large, predominantly [111] oriented grains.[18] Third, the alumina grows in the amorphous state.[18] Fourth, the oxidation time is critical for producing SDT junctions with good SP properties.[19] In particular, overoxidation of the barrier leads to the formation of cobalt oxide, which destroys the spin polarization of the electrons in the ferromagnet, whereas unoxidized aluminum leads to the presence of unpolarized electrons in the tunneling barrier.

The first two features are incorporated into our structural model by stacking fcc (111) Co layers. The MTJ's are produced by depositing a few tens of monolayers of aluminum film on top of the crystalline ferromagnet layer followed by thermal- or plasma-assisted oxidation to create the alumina tunneling barrier (see, e.g., Ref. 20). Therefore it is reasonable to assume that the cobalt film (deposited at the beginning of the manufacturing cycle) serves as a base with the bulk lattice parameter fixed in the plane parallel to the interface. The alumina is then formed by adjusting its structure to that of cobalt during the course of oxidation. The third feature, i.e., the amorphous state of alumina cannot be directly modelled at present by first-principles methods due to the large number of atoms needed in the simulation cell. Therefore we consider crystalline α-Al_2O_3 with the [0001] orientation on top of fcc (111) Co, as a first step in modeling a realistic $Co/Al_2O_3/Co$ MTJ. We have carefully studied all the possibilities of relative crystallographic alignments of cobalt and alumina and identified the crystal structure with the minimal lattice mismatch. The lateral dimensions of our supercell correspond to a 2×2 surface unit cell of the (111) plane of fcc cobalt with the theoretical lattice parameter $a = 5.057$ Å . The experimental lattice parameter a of corundum is 4.759 Å which results in a 6% lattice mismatch.

Obviously, the fourth factor, i.e., importance of the oxidation time, points to the necessity to investigate the effects of different terminations of the $Co/Al_2O_3/Co$ MTJ: in the case of underoxidation we have an aluminum terminated interface, in the overoxidized case there is an abundance of oxygen at the interface. There are numerous possibilities for the termination of the alumina slab but we decided to consider the two limiting cases of oxygen-rich and aluminum-rich interfaces in order to get a feeling of the influence of oxidation on the SDT device characteristics. For both the O- and Al-terminated interfaces we use a seven-layer-thick cobalt slab with four cobalt atoms per layer (28 cobalt atoms in total) and a seven-layer-thick alumina slab, the composition of the latter being dependent on the termination.

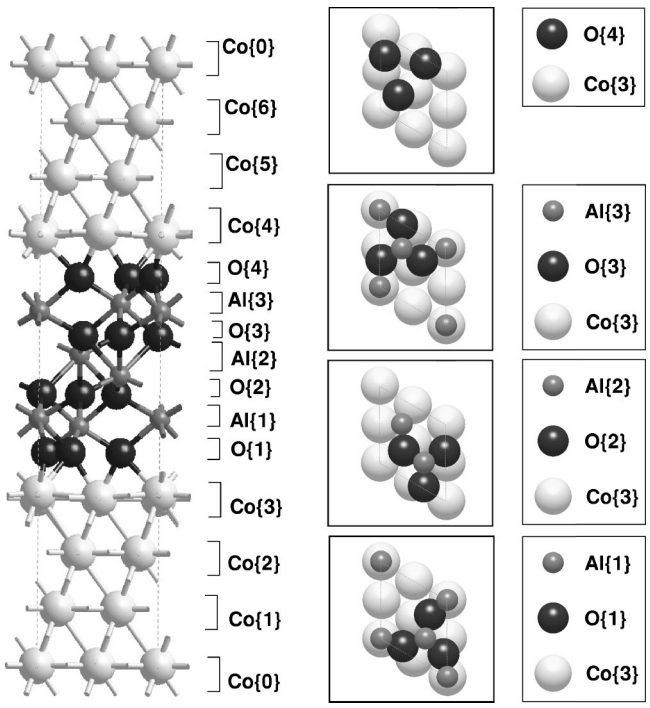

FIG. 1. The relaxed structure of the O-terminated MTJ. The left-hand panel is a side view of the supercell, the right-hand panel is a layer-by-layer projection of the structure onto the (0001) plane using the Co{3} layer as reference. The layers are labeled by the chemical symbol of the element comprising the layer and are numbered from the bottom to the top.

The O-terminated interface supercell, Fig. 1, consists of four oxygen layers of alumina (O{1}, O{2}, O{3}, O{4}) with $4\times3=12$ oxygen atoms in total, plus three Al layers (Al{1}, Al{2}, Al{3}) with $3\times2=6$ Al atoms resulting in total composition of $28Co+12O+6Al=46$ atoms in the unit cell. The symmetry of the O-terminated interface is P-3 (trigonal-hexagonal plus inversion). The Al-terminated interface, Fig. 2, consists of four Al layers of alumina (Al{1}, Al{2}, Al{3}, Al{4}) with $4\times2=8$ atoms of aluminum plus three O layers (O{1}, O{2}, O{3}) with $3\times3=9$ atoms of oxygen resulting in the total composition of $28Co+8Al+9O=45$ atoms in the unit cell. The symmetry of the Al-terminated interface is P123 (trigonal-hexagonal plus reflection). Both the O- and Al-terminated interfaces are not in stoichiometric compositions. We note that the structure of Co and the arrangement of the aluminum atoms at the Al-terminated interface is different from that considered in Ref. 21. We found that the position of the Al atoms above the hollow sites of the interfacial Co layer is energetically more favorable than the structure where the positions of the Al atoms are directly above

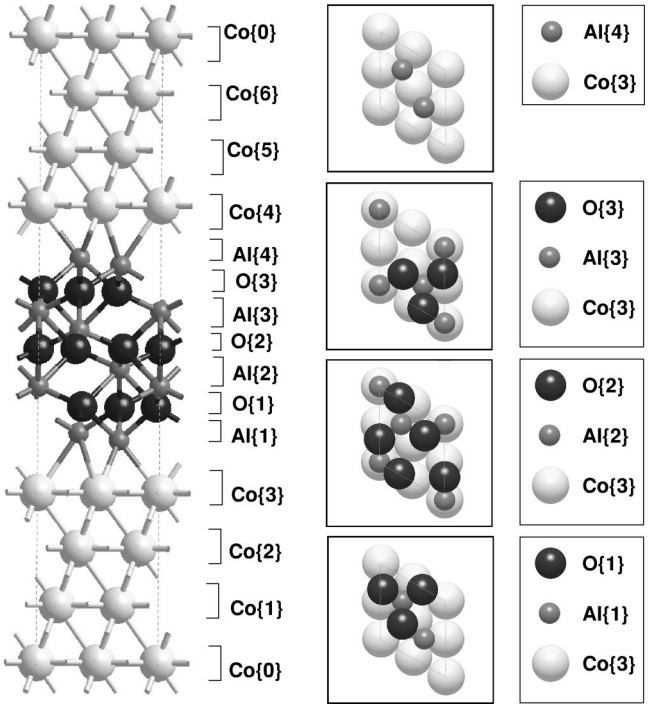

FIG. 2. The relaxed structure of the Al-terminated MTJ. The left-hand panel is a side view of the supercell, the right-hand panel is a layer by layer projection of the structure onto the (0001) plane using the Co{3} layer as reference. The layers are labeled by the chemical symbol of the element comprising the layer and are numbered from the bottom to the top.

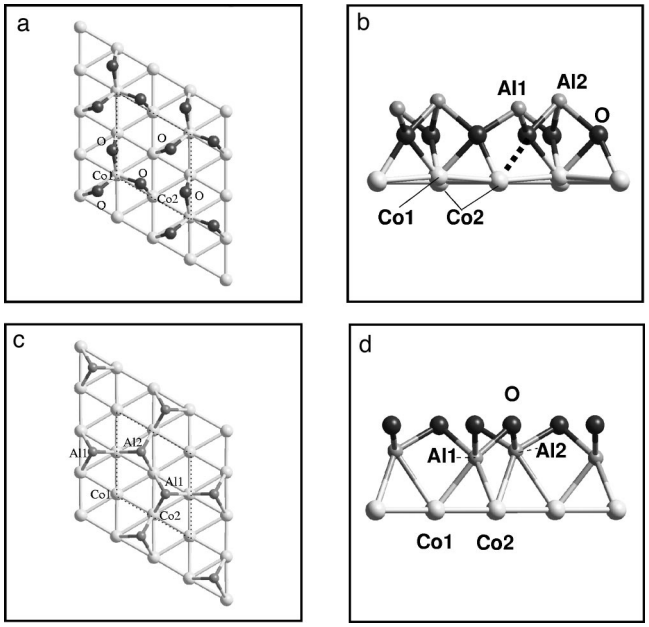

FIG. 3. Top panels: bonding geometry of the O-terminated MTJ: (a) top view of the Co{3} and O{1} layers, (b) side view of the Co{3}, O{1} and Al{1} layers. The dashed bond in the side view (b) shows the bond between O and back Co2 atoms. Bottom panels: bonding geometry of the Al-terminated MTJ: (c) top view of the Co{3} and Al{1} layers, (d) side view of the Co{3}, Al{1} and O{1} layers.

the Co atoms as was assumed in Ref. 21.

Spin-polarized plane-wave pseudopotential calculations of the geometry and total energy within the generalized gradient approximation[22] and with the use of Vanderbilt ultrasoft pseudopotentials[23] were made with the code *CASTEP*.[16] The plane-wave energy cutoff E_{cut} was chosen as 300 eV and the Monkhorst-Pack *k*-space sampling scheme was used with two *k* points in the irreducible wedge of Brillouin zone. Tests were performed with a larger cutoff and denser *k*-point sampling to check that these particular values guarantee convergence of the atomic forces to better than 0.1 eV/Å .

In order to determine the relaxed structure of the MTJ, it was critical to perform an optimization of all the internal coordinates of the atoms as well as the height of the unit cell. The constraints of fixed lateral cell dimensions and frozen three middle layers of cobalt were imposed in order to simulate the experimental conditions of the growth on the cobalt base. For a given cell size the atomic internal degrees of freedom were relaxed to give the minimum-energy structure. The cell size was then varied and the relaxed structure was deduced from the minimum of the resultant binding energy curve. The relaxed structures are shown in Fig. 1 for the O-terminated interface and in Fig. 2 for the Al-terminated interface. In order to make the bonding configurations at the interface clearer we have displayed ball and stick models of the interface regions composed of Co{3}, O{1} layers for the O-terminated interface in the top panel of Fig. 3 and Co{3}, Al{1} layers for the Al- terminated interface in the bottom panel of Fig. 3 (the side views contain also an additional layer of alumina, Al{1} and O{1} for O and Al terminations, respectively).

A. O-terminated interface

We see from the top panels in Fig. 3 that at the O-terminated interface the three oxygen atoms in the O{1} layer participate in bonding with the four cobalt atoms in the Co{3} layer. Since the O-terminated interface possesses P-3 symmetry all three oxygen atoms are equivalent so we label them O. Looking at the cobalt side, the four cobalt atoms are divided into the three equivalent atoms Co2 and the single atom Co1 which is centered on the axis of symmetry. This Co1 atom forms three equivalent bonds with surrounding O atoms with a bond length $R(\text{Co1-O}) = 2.12$ Å, whereas each of the other three Co2 atoms forms a bond with a single oxygen with a bond length $R(\text{Co2-O}) = 1.97$ Å. This difference in bond number between the Co sites causes the O-terminated interface to ripple by 10%. From the Al_2O_3 side of the interface, every oxygen atom has two inequivalent bonds $R(\text{Co1-O})$ and $R(\text{Co2-O})$ with the Co1 and Co2 atoms plus two inequivalent bonds with the aluminum atoms Al1 and Al2 in the layer Al{1} [$R(\text{Al1-O}) = 1.84$ Å and $R(\text{Al2-O}) = 1.95$ Å]. In both interface terminations Al1 labels the aluminum atom within the first alumina layer Al{1} that is closest to cobalt, whereas Al2 labels the aluminum atom within the same Al{1} layer, but shifted along the *z* direction towards the alumina side, see Fig. 3. The average Co-O bond length of 2.04 Å is within 5% of that in bulk CoO.[24]

The general topology of the atomic relaxations at the O-terminated interface can be interpreted in terms of the surfacelike behavior of the individual cobalt and alumina slabs but with some modification due to the mutual interaction of the two surfaces. The three Co2 atoms of the Co{1} layer undergo a substantial contraction of 0.12 Å towards the core

of the metal, although as we have seen the single Co1 atom moves up in the opposite direction by 0.05 Å towards the alumina as a result of its threefold bonding with the O atoms in the O{1} layer. The extent of the Co{1} contraction is almost the same as that of a free-standing Co fcc (001) surface, the latter relaxing homogeneously since all the surface atoms are equivalent.

The features of the atomic rearrangements from the alumina side of the interface are a rotation of the triangle comprising the O atoms in the O{1} layer by 10° with the *z*-directed rotational axis centered on the Al2 atom above the triangle, and a movement of the Al1 and Al2 atoms of the Al{1} layer in the *z* direction towards each other [see the change of $\Delta z(\text{Al2-Al1}) = 0.28$ Å with respect to the bulk value of 0.54 Å]. The rotation of the O triangle is also observed for the case of the O-terminated α-Al_2O_3 surface and this relaxation is explained in terms of electrostatic forces.[25]

B. Al-terminated interface

At the Al-terminated interface two aluminum atoms in the Al{1} layer interact with the four cobalt atoms in the Co{3} layer as shown in the lower panels of Fig. 3. Atom Al1 occupies the fcc hollow site in the next layer, and the Al2 atom is at the hcp hollow site (these positions are identified as hcp or fcc with respect to in-plane coordinate stacking). The Co1 atom does not have any bonds with the interfacial Al{1} layer, and each of the three equivalent Co2 atoms is bonded to one Al1 atom with a bond length 2.40 Å and to one Al2 atom with a bond length 2.58 Å . From the alumina side of the interface one Al1 atom is bonded to three Co2 atoms and the Al2 atom also has three Co2 nearest neighbors. The $P123$ symmetry of the cell includes a threefold rotation in addition to reflection. All the three Al-Co bonds originating from a particular Al atom are identical, the Co2-Al2 bond lengths being the longest. Interestingly, the average value of the Co-Al bond lengths, namely 2.49 Å, is equal to the average Al-Co bond lengths in CoAl intermetallic compound.[26]

Examining the interface relaxation of the Co slab we find almost the same picture of surface-like behavior of the first two cobalt layers as we found for the O-terminated interface, i.e., a contraction of the Co{3} layer by 0.11 Å and a contraction of the Co{2} layer by 0.06 Å . However, all the four Co atoms in the Co{1} layer have the same value of contraction towards the bulk, which is in contrast to the case of the O-terminated interface. The relaxation of the alumina slab at the interface is minimal. The O{1} layer remains unchanged with no rotations or visible attraction to the Co{3} layer. The only important feature of the alumina slab relaxation is the reduction of $\Delta z(\text{Al2-Al1})$ causing the Al1 and Al2 atoms to lie almost in the same plane. This is in sharp contrast to the Al-terminated surface of α-alumina where there is a strong effective repulsion between the Al1 and Al2 atoms. This repulsion occurs for those geometries where the Al2 atom lies very close to the O{1} plane. The two-aluminum-atom termination is nonstoichiometric and the system tries to restore stoichiometry by repelling the unnecessary atom out of the system.

III. ELECTRONIC STRUCTURE

Using the relaxed atomic structure, we calculated the spin-polarized electronic structure of both the O- and Al-terminated $Co/Al_2O_3/Co$ MTJ using the LMTO method[17] within the atomic sphere approximation (ASA). The LMTO method makes use of the local spin-density approximation (LSDA) to the density-functional theory. In general, spin-polarized generalized gradient approximation (GGA) is more accurate than LSDA in atomic structure and energetics, but the difference between former and latter in electronic properties of solid-state systems is relatively small.[27] We note that both methods suffer in equal extent from the well-known failing of canonical DFT to reproduce correctly the band gaps of semiconductors and insulators as well as the properties of the excited states. The radii of the atom-centered spheres were determined by tracing the potential resulting from the superposition of neutral-atom potentials along the lines connecting nearest-neighbor atoms in order to find the saddle points.[17] For a given atom, the distance to the closest saddle point was taken as the radius of the sphere. The ASA radii were then obtained by inflating the atom-centered spheres until they fill the volume of the unit cell. In order to reduce the overlap between the atom-centered spheres, we introduced empty interstitial spheres (17 for the O-terminated and 12 for the Al-terminated interface). Their positions were chosen to belong to the trigonal P-3 and P123 symmetry group for the O- and Al-terminated Co/Al_2O_3 unit cells, respectively. The resulting overlap between the atom-centered spheres and empty spheres was found to be less than 18%. The self-consistent calculations were performed by taking into account the muffin-tin orbitals of the *s*, *p*, and *d* angular momenta and using a grid of 16 k points in the irreducible wedge of Brillouin zone. A tolerance in the total energy of 10^{-5} Ry was achieved. The electron densities of states (DOS), the charge density and the spin density were obtained with a grid of 76 irreducible *k* points.

A. O-terminated interface

The resulting spin- and layer-dependent DOS for the O-terminated interface are shown in the left-hand panel of Fig. 4. The top two panels (a) and (b) display the LDOS of the O{2} and Al{2} layers in the middle of the oxide. We found that these LDOS are very similar to those obtained for the bulk α-Al_2O_3.[28,29] Like in the bulk alumina, the valence band, which lies in the energy window from -10 to -3.5 eV, is composed of the O $2p$ orbitals hybridized with the Al $3s$, $3p$, and $3d$ orbitals. The bottom part of the valence band consists of the O-Al bonding states and the top part of the valence band is formed of the O-Al nonbonding states. We note that there is a lower valence band of the O $2s$ orbitals which is separated by a gap of 8.7 eV from the upper O $2p$ valence band and is located below the displayed energy interval. The conduction band lies at energies above 2 eV, its bottom part being represented mainly by *s* orbitals of Al mixed with *p* and *s* orbitals of O. In the bulk α-Al_2O_3 the valence and the conduction bands are separated by a band gap which is, according to our results, equal to 6.2 eV at the Γ point. Although this value is less than the experimental band gap of 8.8 eV (Ref. 30) as a result of using the local-density approximation (LDA), it is in good agreement with

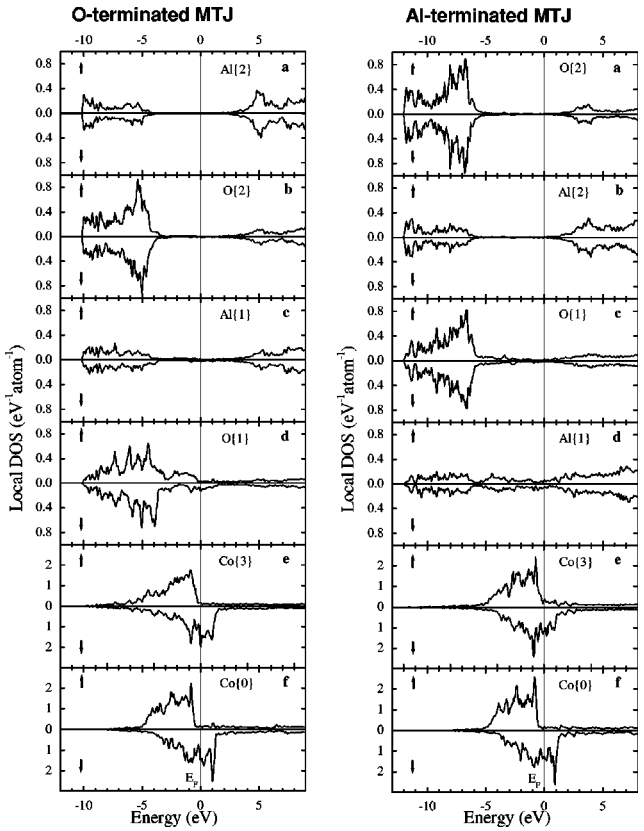

FIG. 4. Layer-projected spin-dependent densities of states of the O-terminated $Co/Al_2O_3/Co$ MTJ (left-hand panel) and Al-terminated $Co/Al_2O_3/Co$ MTJ (right-hand panel) as a function of electron energy. The majority- and minority-spin densities of states are shown by arrows pointed up and down respectively. The Fermi level is denoted by the vertical line.

an all-electron full-potential LDA calculation.[31] In the presence of the interface with the Co metal the LDOS within the band gap of alumina (layers O{2} and Al{2}) is not exactly zero. At energies within the band gap, the electronic states of the Co metal propagate into the insulator barrier, decaying roughly exponentially with the distance in the oxide layer. These metal-induced states are spin-polarized and are responsible for the spin-dependent tunneling.[3] The Fermi level lies within the band gap of Al_2O_3 at about 3.5 eV above the top of the valence band.

The DOS of the inner Co{0} layer [panel (f)] is similar to the bulk DOS of fcc Co[32]. The magnetic moment of this Co{0} layer, $1.72\mu_B$, is slightly enhanced compared to the theoretical bulk value of $1.62\mu_B$ due to the finite thickness of the Co slab. As is evident from the figure, the *d* band of the majority-spin electrons is filled and the Fermi level lies within the majority *sp* band. On the other hand, the *d* band of the minority-spin electrons is not completely filled and the Fermi level lies within the *d* band. The exchange splitting of the *d* bands is about 1.8 eV. Although these features remain unchanged in the DOS of the interfacial Co{3} layer, it differs from the DOS of the bulk Co{0} layer as a result of the reduced symmetry of the interface and the covalent bonding between this Co{3} layer and the adjacent oxygen O{1} layer of Al_2O_3. In particular, the *d* band of the interfacial Co{3} layer is smeared out compared to the bulk [compare Figs. 4(e) and (f)], and the electronic states extend down to -10 eV as a result of the bonding with oxygen. This bonding does not, however, quench the interface magnetism, the magnetic moment of the interfacial Co{3} layer being $1.68\mu_B$. This is different from what was found for the $Co/HfO_2(001)$ interface,[33] where the majority *d* band of the interfacial Co layer was not completely occupied and consequently the magnetic moment of this layer was strongly reduced compared to the bulk.

The DOS of the oxygen O{1} layer at the interface is very different from that in the 'bulk' of alumina O{2} layer [compare Figs. 4(d) and (a)]. This difference is the result of the covalent bonding between the $2p$ orbitals of oxygen and the $3d$ orbitals of cobalt. The pronounced four peaks in the energy interval between -3 and -8 eV for both the majority- and minority-spin electrons are associated with the formation of the bonding states. These bonding states are split by about 0.3 eV, which is much less than the exchange splitting of the *d* bands of the interfacial Co{1} layer, being about 1.8 eV. This is due to the fact that the Co *d* bands lie at higher energies and the splitting of the bonding states occurs via a second-order perturbation contribution. In addition to the bonding levels below the *d* bands, the oxygen DOS displays a broad band of antibonding states that extends up to about 2 eV above the Fermi energy. The exchange splitting of the *d* bands of Co and the bonding between the *d* orbitals of Co and the *p* orbitals of O induce a splitting of these antibonding states. Contrary to the bonding states, this splitting is large, mirroring the exchange splitting of the surface Co *d* states. The antibonding states are almost fully occupied for the majority spins and are partly occupied for the minority spins. This leads to an induced magnetic moment of $0.07\mu_B$ on the oxygen sites. The local density of states (LDOS) at the Fermi energy is larger for the minority-spin electrons as compared to the minority-spin electrons, i.e., the spin polarization in the density of states at the Fermi energy is negative. We note that this is opposite to the result obtained for the oxygen monolayer deposited on the surface of an Fe (001) slab, where the strong exchange splitting resulted in a positive spin polarization on the oxygen.[34]

The DOS of the Al{1} layer adjacent to the interfacial O{1} layer does not differ significantly from the DOS of the Al{2} layer in the bulk of alumina [compare panels (c) and (a)]. Although a trace of the antibonding Co-O states is still visible at the energies within the band gap, the bonding between the Al and O dominates in the LDOS formation within this layer.

Figure 5 shows charge-density and spin-density contours of the Co/Al_2O_3 system in the (100) Miller plane of the supercell. As evident from the left panel in Fig. 5, the O atom at the interface shares the charge with the two interfacial Co1 and Co2 atoms (the labels of the atoms and geometry of the bonding are explained in Sec. II, see also Fig. 3). This partial localization of the electron density in the region between the atoms is evidence of the covalent character of the Co-O bonding. As already mentioned in Sec. II, the strongest covalent bonding is between the Co2 and O atoms which have the smallest bond length of 1.97 Å . The Co1 atom at the interface has much weaker bonding with O. As is seen from the left panel in Fig. 5, there is little electron charge propagating from the O atom to the nearest Al1 atom and the region between them is characterized by a very low

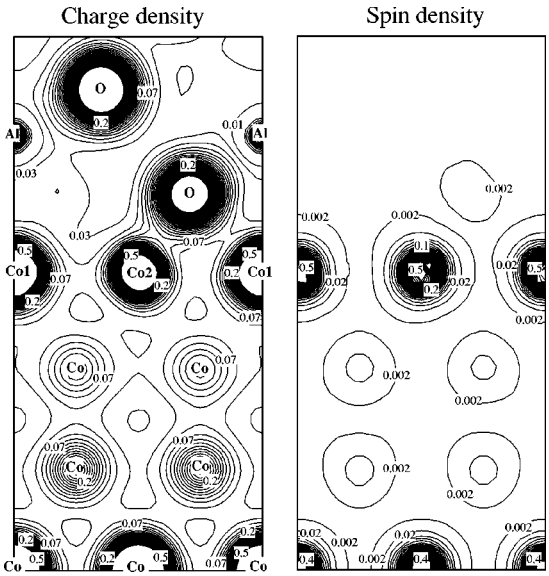

FIG. 5. Charge-density and spin density contours (in atomic units) of the O-terminated $Co/Al_2O_3/Co$ MTJ in the (100) Miller plane of the supercell shown in Fig. 1.

charge density. This fact and the sizeable charge transfer between the Al and O (Ref. 35) demonstrate the dominance of the ionic character in the Al-O bond, which is known from previous studies of bulk alumina.[30,36,37]

The spin density in Fig. 5 is characterized by a large positive contribution from the Co atoms. This is not surprising because of the sizeable ferromagnetically aligned magnetic moments of the Co atoms. The spin density, which is almost spherical on the bulk Co atoms, is slightly distorted at the interface due to the bonding with the adjacent O layer. As was discussed above, the interfacial oxygen atom acquires a small magnetic moment which is aligned parallel to the magnetic moment of Co. This is reflected in a small positive spin cloud around the O atom in Fig. 5. As is seen from Fig. 5, the spin density on all the other atoms of alumina is zero.

B. Al-terminated interface

The electronic and magnetic properties of the Al-terminated interface differ from those of the O-terminated one. The main difference comes from the fact that in this case the interfacial Al{1} layer can be considered as the termination of a metal substrate comprising the Co metal layer and the Al monolayer. This is evident from the right-hand panel in Fig. 4 which shows the spin- and layer-dependent DOS of the Al-terminated Co/Al_2O_3 interface: the LDOS of the interfacial Al{1} layer is sizeable at the Fermi energy which is typical for metals [panel (d)]. Like in bulk alumina, the interfacial Al{1} layer has a sizeable positive charge due to the charge transfer to the adjacent O{1} layer.[35] This positive charge is screened very quickly within the Co layer. According to our LMTO results, the interfacial Co{3} layer acquires a sizeable negative charge of about $-0.2|e|$ per atom.[35] This results in the reduction of the average magnetic moment within this Co{3} layer down to approximately $1.15\mu_B$ per atom. As can be seen from panel (e), the Fermi level lies above the majority *d* bands and the reduction in the magnetic moment is mainly due to the minority *d* band filling [compare with the bulk density of states shown in panel (f)]. The DOS of the oxygen and aluminum layers within the interior alumina are qualitatively similar to those obtained for the O-terminated interface [compare panels (a) and (b) in Fig. 4]. There is, however, a difference in the position of the Fermi energy: in the case of the Al-terminated interface it is shifted towards the bottom of the conduction band. As can be seen from panel (d), the SP of the LDOS at the Fermi level on the interfacial Al{1} layer is slightly negative which is opposite to what was found in Ref. 21. This result is a consequence of the different atomic structure at the interface considered in the present paper.

C. Relevance to spin-dependent tunneling

Although in the present paper we do not evaluate the conductance of the $Co/Al_2O_3/Co$ junction, some conclusions about the mechanism of spin-dependent tunneling can be made based on the LDOS consideration. The quantity that is relevant to the tunneling is the LDOS at the Fermi energy within the barrier. This quantity characterizes the decay of the evanescent metal-induced electronic states within the band gap of alumina and could therefore be used for elucidating the factors responsible for the spin polarization of the tunneling current. The LDOS in the alumina within the Co/Al_2O_3 superlattice decays exponentially inside the insulator. For the case of the 7-monolayer (ML) alumina barrier which we have used for geometry optimization and electronic structure calculations reported above, the LDOS could be examined up to 4 ML's from the interface due to the reflection or inversion symmetry of the unit cell. We have therefore performed an additional LMTO calculation in which the thickness of the α-alumina insulating barrier in the O-terminated Co/Al_2O_3 structure was increased by 12 extra monolayers of alumina (i.e., by the size of the conventional unit cell of bulk alumina). The conventional unit cell was chosen with the bulk geometry, optimized at the fixed lattice parameter $a=5.057$ Å , as was described earlier.

The resulting layer resolved LDOS of the extended O-terminated Co/Al_2O_3 structure for the layers O{1}, Al{1}, O{2}, Al{2} is almost identical to that obtained for the case of the seven layer alumina slab shown in Fig. 4. In particular, we find the induced exchange splitting of the electronic states on the interface oxygen sites and the negative spin polarization in the LDOS of the interfacial O{1} layer at the Fermi energy [similar to those presented in the left-hand panel (d) of Fig. 4]. It is important to note that the increased thickness of the alumina does not change the position of the Fermi level with respect to the band gap, as it is determined by the dipole layer formed in the close vicinity of the interface due to the charge transfer between the metal and the insulator.[38]

Figure 6(a) illustrates the behavior of the LDOS at the Fermi energy for the majority and minority spin electrons as a function of the distance from the interface Co layer. Evidently, the LDOS decreases exponentially with the distance. Although the minority LDOS is larger at distances near the interface, it decays more rapidly as compared to the majority LDOS. Eventually the majority LDOS starts to dominate over the minority LDOS resulting in the positive SP. This

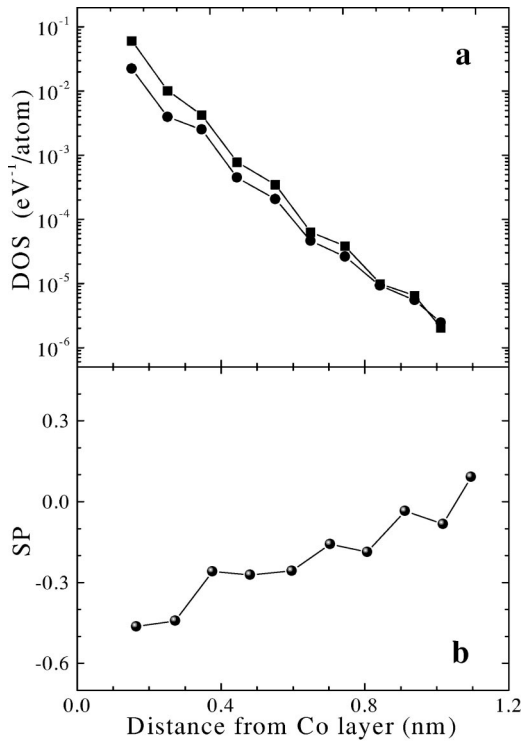

FIG. 6. The local density of states at the Fermi energy for the majority- (circles) and minority- (squares) spin electrons (a) and the spin polarization of the DOS (b) as a function of the distance from the interface Co layer.

can be seen from Fig. 6(b), which shows the SP of the LDOS at the Fermi level as a function of the distance from the interface Co layer. The SP is defined by $(D_\uparrow - D_\downarrow)/(D_\uparrow + D_\downarrow)$, where $D_\uparrow$ and $D_\downarrow$ are the LDOS for the majority and minority spins, respectively. As is evident from Fig. 6(b), the layer-averaged SP increases gradually without showing a tendency for saturation.

In order to obtain quantitative information about the behavior of the LDOS within the barrier, we fitted the two curves presented in Fig. 6(a) by the exponential function $A\exp(-2\kappa z)$, where A is the constant, z is the distance from the interface, and κ is the decay constant. We found that $\kappa_\uparrow = 0.48$ Å $^{-1}$ and $\kappa_\downarrow = 0.54$ Å $^{-1}$ for the majority and minority spins, respectively. This corresponds to the decay lengths $l_\uparrow = 1.04$ Å and $l_\downarrow = 0.93$ Å . The decay constants determine the height of the effective potential barrier $U = \hbar^2\kappa^2/(2m^\star)$. Assuming that the effective electron mass $m^\star$ is equal to the free-electron mass, we obtain $U_\uparrow = 0.88$ eV and $U_\downarrow = 1.11$ eV. It is not surprising that these values of the barrier height are lower than the values of 2–2.5 eV extracted from experimental data (see, e.g., Ref. 2), because LDA underestimates the band gap in insulators.

The fact that $U_\uparrow < U_\downarrow$ implies that in the limit of large insulator thickness the tunneling current should become 100% positive spin polarized. Such a behavior was predicted by theory for epitaxially grown iron/semiconductor tunnel junctions.[12] In our case this conclusion might be precocious since the analysis is based on the LDOS at the Fermi energy. It is well known that electronic states which correspond to different transverse momenta decay in the barrier with different decay lengths. In the case of alumina which has a minimum direct band gap at the Γ point, the electronic states with zero transverse momentum have the lowest effective barrier height and consequently the longest decay length. In addition to this, as was shown in Ref. 12, the bands which are characterized by different symmetry, i.e., associated with different angular character within the barrier, can have unequal decay lengths. We conclude therefore that in order to fully understand the factors controlling the SP, further calculations are necessary, which include the explicit evaluation of the conductance and its analysis in terms of contributions from the states with different transverse momenta and orbital characters.

IV. CONCLUSIONS

The major focus of this work was to understand the atomic structure and electronic properties of the cobalt/alumina MTJ from first principles. In order to make the problem tractable we considered crystalline α-alumina with the [0001] orientation on top of the (111) plane of fcc cobalt within a supercell geometry. Since experiments showed the critical influence of the oxidation time on the value of the TMR we considered two limiting cases of interface termination, namely oxygen rich and aluminum rich.

We found that the relaxed energy structure of the O-terminated $Co/Al_2O_3/Co$ tunnel junction has an average Co-O bond length of 2.04 Å which is within 5% of that in bulk CoO. The threefold bonding of the single Co1 atom results in the rippling of the Co{3} interfacial plane, see Figs. 1 and 3. The changes in the alumina slab are similar to the relaxation of the O-terminated surface of α-alumina, that is a rotation of the triangle of the O atoms by 10° in the O{1} layer and a contraction of the height difference between the Al1 and Al2 atoms from a bulk value of 0.54 to 0.28 Å . The relaxed structure of the Al-terminated MTJ is characterized by the average Co-Al bond length of 2.49 Å compared to 2.48 Å in bulk CoAl.

The electronic structure of the O-terminated interface is affected by the covalent bonding between the $2p$ orbitals of oxygen and the $3d$ orbitals of cobalt. We found that this bonding does not quench the surface magnetism, the magnetic moment of the interfacial Co{3} layer $1.68\mu_B$ being almost unchanged compared to that of bulk Co{0} layer. The hybridization of the Co $3d$ states and the O $2p$ states and the strong exchange splitting of the former result in the exchange-split bonding and antibonding oxygen states and induces a magnetic moment of $0.07\mu_B$ on the interfacial oxygen atoms. The electronic and magnetic properties of the Al-terminated interface are characterized by metallic behavior of the interfacial Al atoms which display a sizeable DOS at the Fermi energy. We found that these Al atoms interact in ionic fashion with the adjacent oxygen atoms and acquire an appreciable positive charge as a result of electron transfer to oxygen. This positive charge is screened by the interfacial Co{3} layer. The screening is accompanied by the a negative charge and a reduction of the magnetic moment to $1.15\mu_B$ per atom for this Co{3} layer.

Semiquantitative conclusions about spin-dependent tunneling were made by performing electronic structure calculations of an extended O-terminated Co/Al_2O_3 supercell, containing 19 layers of Al_2O_3. We found that the LDOS at

the Fermi energy decays exponentially with distance from the interface into the alumina, the average decay length being larger for the majority-spin electrons than for the minority-spin electrons. Although the spin polarization (SP) of the LDOS is negative within the first few monolayers of alumina, it gradually increases and eventually becomes positive at a distance of 10 Å .

In order to fully understand the factors controlling the SP of the tunneling current, tunneling conductance must be evaluated explicitly and an analysis made in terms of contributions from states with different transverse momenta and orbital characters. The influence of the amorphous nature of the insulating alumina layer must also be addressed which requires interatomic potentials that are capable of simulating the atomic arrangements at the ferromagnet/alumina interfaces. As a step in this direction, the results of the current work will be analyzed further in a subsequent paper by focussing on the character of the bonding at the cobalt/alumina interface. A final paper will study the spin-dependent tunneling conductance using the structural information presented here.

ACKNOWLEDGMENTS

The authors wish to thank V. M. Burlakov, M. W. Finnis, D. J. Srolovitz, A. P. Sutton, and H. Wadley for stimulating discussions. I.I.O. thanks DARPA for the financial support under Contract No. N00014-97-1-G015. E.Yu.T. thanks Hewlett Packard Laboratories, Palo Alto for the financial support through a collaborative research program. The calculations were performed in the Materials Modelling Laboratory at the Department of Materials and in the Oxford Supercomputer Center, University of Oxford.

[1] For a recent review, see G.A. Prinz, J. Magn. Magn. Mater. **57**, 200 (1999).
[2] J.S. Moodera, J. Nassar, and G. Mathon, Annu. Rev. Mater. Sci. **29**, 381 (1999).
[3] R. Meservey and P.M. Tedrow, Phys. Rep. **238**, 173 (1994).
[4] M. Julliere, Phys. Lett. **54A**, 225 (1975).
[5] S.S.P. Parkin (unpublished).
[6] J.M. De Teresa, A. Barthelemy, A. Fert, J.P. Contour, R. Lyonnet, F. Montaigne, P. Seneor, and A. Vaures, Phys. Rev. Lett. **82**, 4288 (1999).
[7] J.C. Slonczewski, Phys. Rev. B **39**, 6995 (1989).
[8] S. Zhang and P.M. Levy, Eur. Phys. J. B **10**, 599 (1999).
[9] E.Yu. Tsymbal and D.G. Pettifor, Phys. Rev. B **58**, 432 (1998).
[10] H. Itoh, A. Shibata, T. Kumazaki, J. Inoue, and S. Maekawa, J. Phys. Soc. Jpn. **68**, 1632 (1999).
[11] E.Yu. Tsymbal and D.G. Pettifor, J. Phys.: Condens. Matter **9**, L411 (1997).
[12] J.M. MacLaren, X.G. Zhang, W.H. Butler, and X. Wang, Phys. Rev. B **59**, 5470 (1999).
[13] G. Dehm, M. Rühle, G. Ding, and R. Raj, Philos. Mag. B **71**, 1111 (1995); G. Gutekunst, J. Mayer, and M. Rühle, Philos. Mag. A **75**, 1329 (1997); **75**, 1357 (1997).
[14] I.G. Batirev, A. Alavi, and M.W. Finnis, Phys. Rev. Lett. **82**, 1510 (1999).
[15] T. Hong, J.R. Smith, and D.J. Srolovitz, Acta Metall. Mater. **43**, 2721 (1995).
[16] M.C. Payne, M.P. Teter, D.C. Allan, T.A. Arias, and J.D. Joannopoulos, Rev. Mod. Phys. **64**, 1045 (1992); *CASTEP* 3.9, academic version, licensed under UKCP-MSI agreement, 1999.
[17] O.K. Andersen, Phys. Rev. B **12**, 3060 (1975); O.K. Andersen, O. Jepsen, and M. Sob, in *Electronic Band Structure and Its Applications*, edited by M. Yussouff (Springer-Verlag, Berlin, 1986); G. Krier, O. Jepsen, A. Burkhart, and O.K. Andersen, The TB-LMTO-ASA Program, Stuttgart, 1995 (unpublished).
[18] X. Portier, A.K. Petford-Long, T.C. Anthony, and J.A. Brug (unpublished).
[19] J.J. Sun, V. Soares, and P.P. Freitas, Appl. Phys. Lett. **74**, 448 (1999).
[20] T. Miyazaki and N. Tezuka, J. Magn. Magn. Mater. **139**, L231 (1995).
[21] D. Nguyen-Manh, E.Yu. Tsymbal, D.G. Pettifor, C. Arcangeli, R. Tank, O.K. Andersen, and A. Pasturel, in *Microscopic Simulation of Interfacial Phenomena in Solids and Liquids*, edited by S.R. Phillpot, P.D. Bristowe, D.G. Stroud, and J.R. Smith, MRS Proceedings No. 492 (Materials Research Society, Pittsburgh, 1998), p. 319.
[22] J.P. Perdew, in *Electronic Structure of Solids '91*, edited by O. Ziesche and H. Eschrig (Akademie-Verlag, Berlin, 1991), p. 11; J.P. Perdew and Y. Wang, Phys. Rev. B **45**, 13 244 (1992).
[23] D. Vanderbilt, Phys. Rev. B **41**, 7892 (1990).
[24] *CRC Handbook of Chemistry and Physics*, edited by D. R. Lide (CRC Press, New York, 1996).
[25] I. Batyrev, A. Alavi, and M.W. Finnis, Faraday Discuss. **114**, 33 (2000).
[26] R. Phillips, J. Zou, A.E. Carlsson, and M. Widom, Phys. Rev. B **49**, 9322 (1994).
[27] I.-H. Lee and R.M. Martin, Phys. Rev. B **56**, 7197 (1997).
[28] B. Holm, R. Ahuja, Y. Yourdshahyan, B. Johansson, and B.I. Lundqvist, Phys. Rev. B **59**, 12 777 (1999).
[29] S.D. Mo and W.Y. Ching, Phys. Rev. B **57**, 15 219 (1998).
[30] R.H. French, J. Am. Ceram. Soc. **73**, 477 (1990).
[31] J.C. Boetter, Phys. Rev. B **55**, 750 (1997).
[32] V.L. Moruzzi, J.F. Janak, and A.R. Williams, *Calculated Electronic Properties of Metals* (Pergamon, New York, 1978).
[33] P.K. de Boer, G.A. de Wijs, and R.A. de Groot, Phys. Rev. B **58**, 15 422 (1998).
[34] E.Yu. Tsymbal, I.I. Oleinik, and D.G. Pettifor, J. Appl. Phys. **87**, 5230 (2000).
[35] The details of the charge redistribution at the Co/Al_2O_3 interfaces will be published in a subsequent paper.
[36] C. Sousa, F. Illas, and G. Pacchioni, J. Chem. Phys. **99**, 6818 (1993).
[37] J. Guo, D.E. Ellix, and D.J. Lam, Phys. Rev. B **45**, 3204 (1992).
[38] G. Bordier and C. Noguera, Phys. Rev. B **44**, 6361 (1991).